Journal of Materials Science & Technology 38 (2020) 189–196

Contents lists available at ScienceDirect

Journal of Materials Science & Technology

journal homepage: www.jmst.org

Research Article

Static and cyclic oxidation of Nb-Cr-V-W-Ta high entropy alloy in air from 600 to 1400 °C

S.K. Varma [a,*], Francelia Sanchez [a], Sabastian Moncayo [a], C.V. Ramana [b]

[a] Department Metallurgical, Materials and Biomaterials Engineering, The University of Texas at El Paso, El Paso, TX, 79968-0520, USA
[b] Center for Advanced Materials Research (CMR), The University of Texas at El Paso, El Paso, TX, 79968-0520, USA

ARTICLE INFO

Article history:
Received 6 August 2019
Received in revised form
10 September 2019
Accepted 10 September 2019
Available online 20 September 2019

Keywords:
High entropy alloys
Nb-Cr-V-W-Ta
Microstructures
Oxidation

ABSTRACT

An oxidation resistance study has been made on Nb-Cr-V-W-Ta high entropy alloy in a range of temperature from 600 to 1400 °C in air. Static oxidation study has been performed for either (a) 12 or 24 h of heating time or (b) 3 or 10 °C/min heating rates to the desired oxidation temperature. Cyclic oxidation study conducted for three and a half days has been conducted at 600, 700, and 800 °C using 12 h of heating cycles. The alloy can withstand the cyclic oxidation process with only a reasonable loss of alloy. The identification of oxides indicates crystals of W and Ta oxides in cylindrical form while Nb and Cr oxides show a nodular or granular morphology at both 1000 and 1200 °C while and additional of oxide of V in whisker forms at 1200 °C.

1. Introduction

A new class of alloys, called high entropy alloy (HEA), have emerged very recently. *HEA is defined as a system containing a minimum of five elements in equiatomic proportion*. Attempts are being made to evolve a high temperature alloy to replace the conventionally used nickel based superalloy. The multicomponent system can make use of many strengthening mechanisms and provide the necessary ductility as well. The source of ductility is the presence of solid solution phase/phases.

Significant advances have been made in the study of HEAs even though the technology is barely a little over a decade old. Numerous reviews can be found in the literature [1–5]. There are attempts being made to evolve medium entropy alloys containing 3 or 4 elements [6] making them as the medium entropy alloys. The presence of a single phase in the alloy due to high configurational entropy is the desirable micro-constituent compared to the intermetallics in some of the high temperature alloys [7,8]. Restrictions of having five elements in equiatomic proportions is being to modified to include minor additions other elements as well [9]. Miracle and Senkov [4] point out to the multi-principal element alloys (MEPAs) and complex concentrated alloys (CCAs). The main premise of the HEAs is to produce single phase alloys providing ductility compared to the alloys containing intermetallic compounds [8–10]. The 4 factors controlling the uniqueness of HEAs include (a) high entropy, (b) diffusional effects, (c) lattice distortions, and (d) properties are not controlled by the components alone. FCC and BCC phases appear to be much more common in HEAs than HCP phases [2].

The yield strength of $Nb_{25}Mo_{25}Ta_{25}W_{25}$ alloy has been determined [11] from room temperature to 1600 °C. The strength drops from low to high temperature ranges from about approximately 1050 to 450 MPa while V addition results in the shift from about 1200 to 450 MPa. It must be noted that alloy has elements with only BCC structures. The high temperature capability, both in terms of retaining high strength and enhanced oxidation resistance, is one of the main reason of exploring HEAs.

The research on refractory metal properties of HEAs has been performed by Senkov and his group [11–16]. The rule of mixtures cannot be applied to the experimental values that have been observed to be 5250 and 3826 MPa respectively which are three times higher than predicted by rule of mixtures [11,13,16]. Authors use atomic size and moduli differences for the elements to explain the discrepancy. However, 50% under compression without fracture is a strong evidence for reasonably good ductility [17–19] HfNbTaTiZr for MoNbTaVW alloys. Microstructural details show the deformation twinning appears to control such ductility in these alloys.

Microstructural stability at elevated temperatures is required property for high temperature applications. It must be noted that HEAs are capable of maintaining high hardness or strength in a

* Corresponding author.
E-mail address: skvarma@utep.edu (S.K. Varma).

https://doi.org/10.1016/j.jmst.2019.09.005
1005-0302/

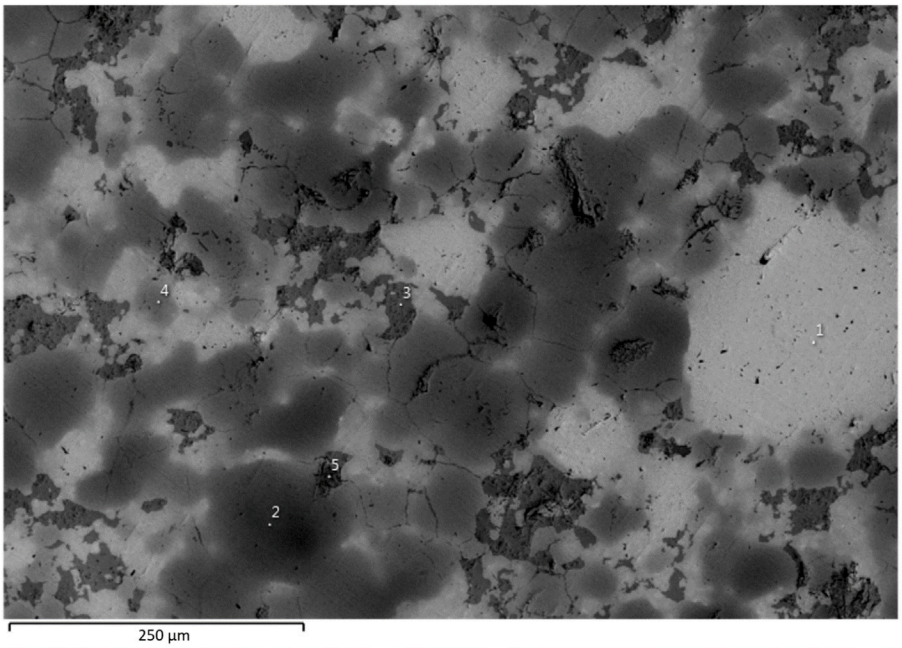

Map Sum Spectrum		1		2		3		4		5	
	At%		At%		At%		At%		At%		At%
Cr	21.7	W	86.1	V	36.1	Cr	48.1	Nb	38.0	Ta	56.8
Nb	21.0	Cr	5.0	Nb	25.9	Ta	23.3	Ta	23.5	V	38.8
W	20.1	V	4.0	Cr	18.8	V	12.9	Cr	16.3	Nb	2.8
Ta	19.1	Nb	2.7	Ta	12.7	Nb	8.5	V	13.6	Cr	1.7
V	18.2	Ta	2.4	W	6.5	W	7.2	W	8.5	W	0.0

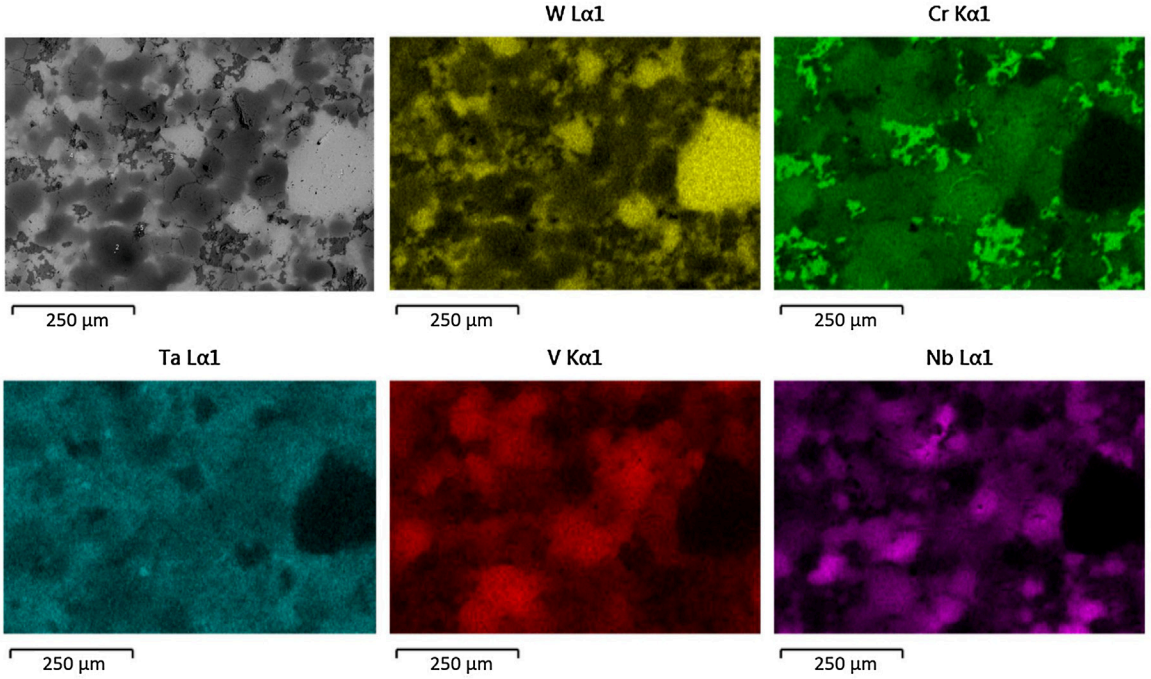

Fig. 1. Microstructure of as received Nb-Cr-V-W-Ta HEA. Table shows the overall composition of the alloy as determined by the EDS in SEM. EDS analysis also shows the compositions of the phases at points marked 1 through 5. Color x-ray mapping identifies the locations of dominant metals in various phases.

high temperature range like $AlCoCr_2FeMo_{0.5}Ni$ while Inconel 718 softens at 800 °C and SKH51 and SUJ2 soften at 600 and 200 °C respectively [20,21]. High temperature stability of high entropy alloys have been attributed to two important thermodynamic features: (a) sluggish diffusion through multi component elements slows the diffusion rate and (b) defects show high stability due to reduction in driving force. Lattice distortion to accommodate many kinds of atoms in unit cells lowers the free energy of the alloys for crystals containing defects. Activation energy for grain growth in CoCrFeMnNi alloys was found to be 321 kJ/mole which

is twice the value for AISI 304 L N steel [22]. This difference can be held responsible for slowing down of the kinetics. High entropies of these alloys also can be held responsible for the resistance to precipitate coarsening. Very small precipitates have been observed from 10 to 100 nm [23,24] for this reason. Thus lowering of the driving force and sluggish diffusion rates contribute significantly to the microstructural stability of these alloys at elevated temperatures as pointed out earlier in the core effects discussion.

There are not many studies that have been performed to evaluate the oxidation resistance, under different atmospheres, of these alloys under both static and cyclic heating conditions. Senkov et al. [8] have observed the oxidation behavior of $NbCrMo_{0.5}Ta_{0.5}TiZr$ alloy in flowing air. $NbCrMo_{0.5}Ta_{0.5}TiZr$ alloy was oxidized at 1273 K for 100 h in flowing air and the instead of a typical parabolic oxidation curve between weight gain per unit area as a function of time they observed an exponent of 0.6 to the time scale. Another important factor observed included the formation of complex oxides but the oxidation layer was confined to a small depth in the alloy. Once again signifying the importance of sluggish diffusion exhibited by HEAs. It must be noted that the alloy contained BCC1, BCC2 and FCC Laves phases in their unoxidized condition and reported values for their volume fractions were 67, 16 and 17% respectively. Although the oxidation layer was found to be nearly 150 μm thick but the oxygen concentration near the surface abruptly drops to zero in much smaller distance increment. Similarly, the elemental distributions in the parent metal was minimally affected and were limited to nm range. The authors concluded that the consideration of HEAs for refractory metals is necessary because present investigations were based on alloys that are brittle at room temperature, oxidation resistance has been confined to below 1000 °C and possess high densities.

Prior to 2009, the pioneer work was performed on oxidation resistance in Nb and Mo based alloys [25–27]. However, the relatively new technology developed by Yeh et al. [28,29] led to the multicomponent system alloys and oxidation resistance is being a subject of exploration by Senkov group since then. Thus far HEAs that have been considered for oxidation resistance include elements like Nb, Ta, Hf, Ti, Zr, Mo, Cr, V, W in various combinations. Reduced number of microconstituents containing multiple elements may be a key to developing a new class of Nb based high oxidation resistant alloys. The purpose of this paper is to present the results of oxidation of Nb-Cr-V-W-Ta HEA alloy in air up to 1400 °C.

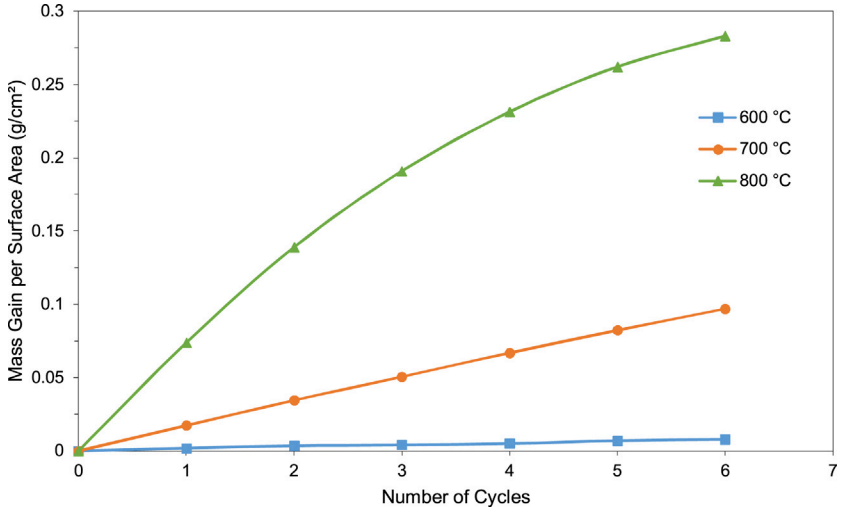

Fig. 2. Cyclic oxidation curves of Nb-Cr-V-W-Ta HEA at 600, 700, and 800 °C. each cycle is for 12 h of heating. Thus the number of cycles can be converted to heating time.

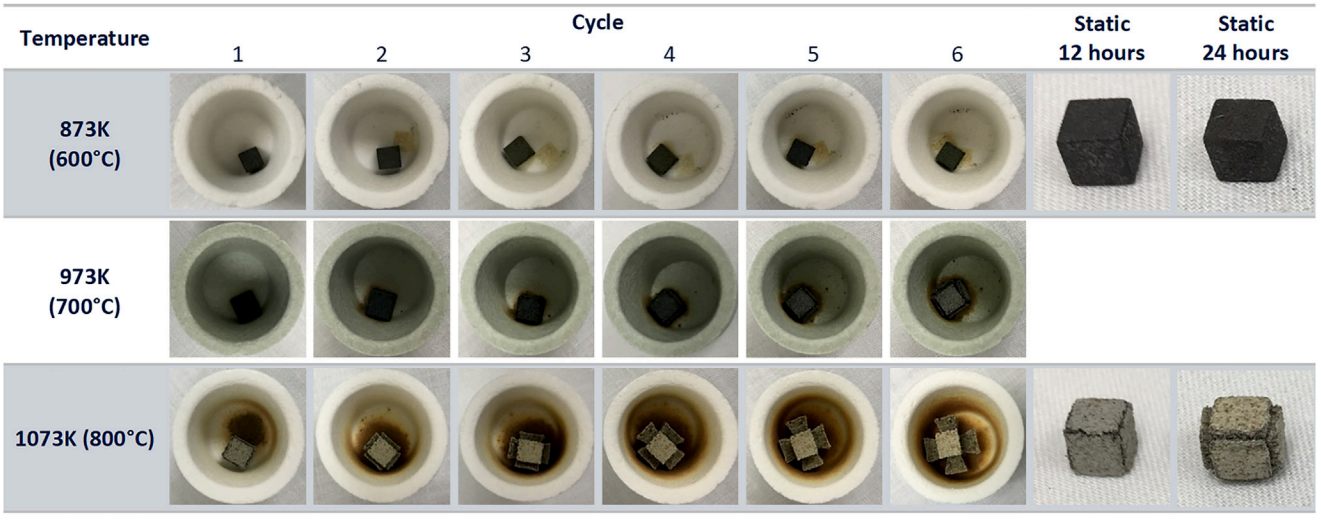

Fig. 3. Samples after 1 through 6 cycles of heating for 12 h at 600, 700, and 800 °C. Samples are also shown for static heating at 600 and 800 °C for 12 and 24 h. Oxide growth at 800 °C is conspicuous.

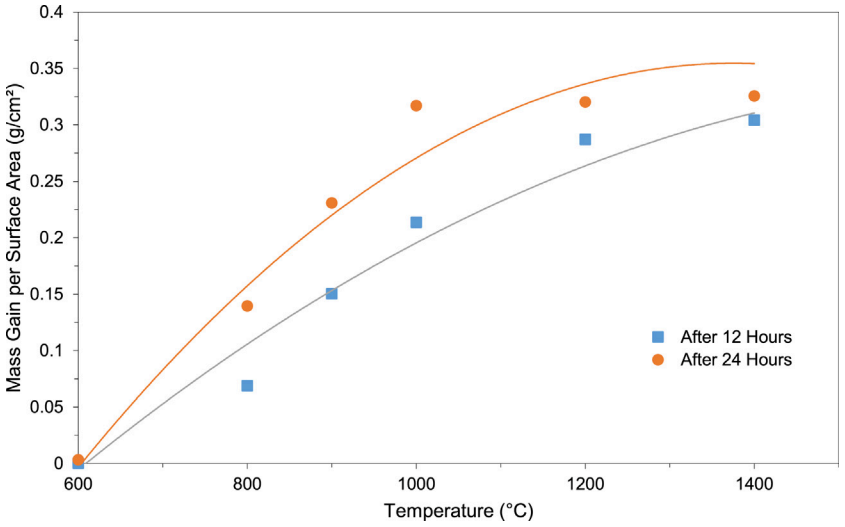

Fig. 4. Static oxidation curves of Nb-Cr-V-W-Ta HEA from 600 to1400 °C for 12 and 24 h.

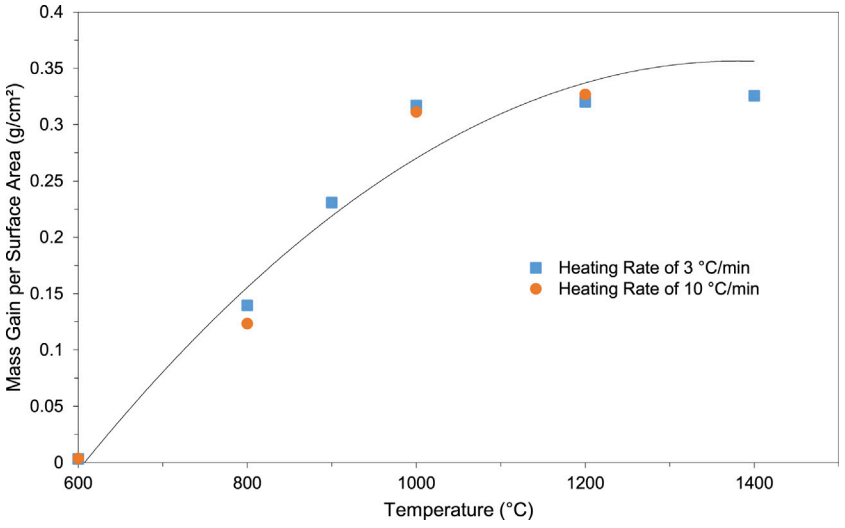

Fig. 5. Static oxidation curves of Nb-Cr-V-W-Ta HEA from 600 to1400 °C at heating rates of 3 and 10 °C to the oxidation temperature. Each heating cycle was for a 24 h duration.

Table 1
Composition of the Trace Elements in Nb-Cr-V-W-Ta HEA in PPM.

Element	PPM	Element	PPM	Element	PPM
Fe	89.8	Si	15.1	Ni	12.6
Mo	13	Ti	<10	Mn	<10
Cu	15.6	Ca	<10	Sn	10
Al	13.4	Mg	10	P	15
Pb	<10	As	<10	Bi	<10
Sb	<10	K	28.3	Na	78.9

2. Experimental

Nb-Cr-V-W-Ta HEA in equiatomic proportion was fabricated by Plasma Materials in California (USA). Alloys were prepared using pure metals of at least 3 nines purity. Samples were cut into 5 × 5x5 cubes using electrical discharge machining (EDM). The compositions of the trace elements provided by the manufacturer is shown in Table 1.

Static and cyclic oxidation study was conducted in a SentroTech furnace with a computer controlled heating and cooling cycle capability. A heating rate of 3 or 10 °C/min was used while the samples were furnace cooled to room temperature. Each heating for the oxidation was executed for either 12 or 24 h at the selected temperature.

Conventional metallographic procedure was used to determine the microstructure. A final 600 grit polishing produced optimum results for observing the microstructures in an SEM. Back scattered electron imaging technique was used in a Hitachi SU 3500 SEM to characterize the microstructures, EDS for composition analysis, and x-ray color mapping allowed the identification for the location of the various elements in the phases. Oxidation products were characterized using a Bruker D8 Discovery using JCPD data.

3. Results and discussion

3.1. As received sample microstructures

The microstructure of the as received (AR) or fabricated sample is shown in Fig. 1. The overall composition of the alloy as determined by EDS can be seen to have the five metals of this study in almost equiatomic proportion as shown by the EDS results in Fig. 1. However, a multiphase microstructure can be seen in the AR

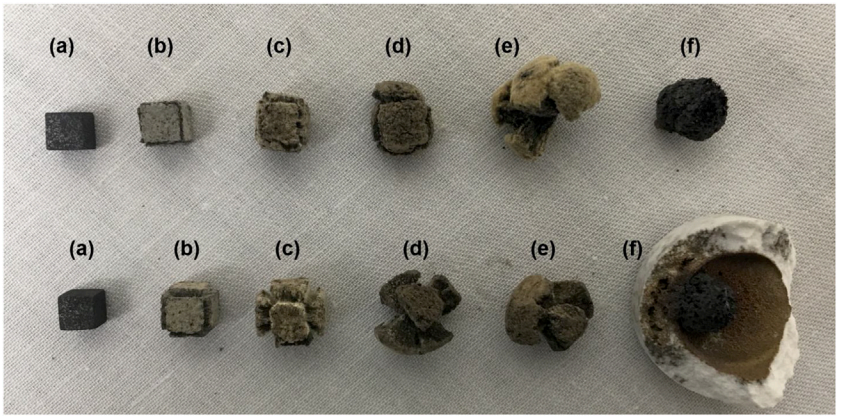

Fig. 6. Samples after oxidation in a range of temperatures from 600 to 1400 °C at a heating rate of 3 °C/min to the oxidation temperature. Figure shows the shapes of the samples after oxidation for 12 and 24 h at the indicated temperatures. a =600 °C, b =800 °C, c =900 °C, d =1000 °C, e =1200 °C, f =1400 °C.

samples of this study. Five areas have been marked in Fig. 1 corresponding to their morphological and compositional differences. The large globules have been shown to contain a W rich phase with, perhaps, Cr and V in solid solutions. Black areas, in small amounts, have been marked as 3 and EDS allows us to identify them as VTa_2, the Laves phase intermetallic compound. The presence of this compound can be verified by any standard V-Ta binary phase diagram. Cloudy or shaded phases can be seen as 2 and 4 areas depending upon their darkness. The compositional analysis in the light cloudy areas are Nb rich (area 4) while the dark areas (area 2) are V-rich. A binary Nb-V phase diagram (from any Standard Metals Handbook) shows the presence of a miscibility gap between them at lower temperatures. Thus it can be concluded that the cloudy microconstituents are mixtures of two phases, either Nb or V-rich. Another distinctly different area has been marked as 5 which the authors attribute them to be a mixture of the Laves phase (VTa_2) and a solid solution of Cr-Ta in a more or less grainy morphological form (gray area). The EDS confirms such observations. Overall, the HEA of this present study contains:

a Area 1 – large white areas consisting of a solid solution of Cr and V in W.
b Area 2 – dark cloudy area is a V-rich phase which is a part of miscibility gap structure.
c Area 3 – black areas are Laves Phase, VTa_2.
d Area 4 - light cloudy area is a Nb-rich phase which is a part of miscibility gap structure.
e Area 5 – Gray or grainy structure which is a mixture of Laves phase and a Cr-Ta solid solution.

3.2. Cyclic oxidation

Cyclic oxidation was performed by subjecting the alloy to various number of cycles of 12 h at 600, 700 and 800 °C. Fig. 2 shows that the mass gain per unit surface area of the alloy increases monotonically up to 6 cycles or three days. The continuous curves shown at 3 selected temperatures clearly indicate there is no cross over meaning that, perhaps, oxidation mechanism is the same at these temperatures. Thus the HEA is capable of sustaining temperatures up to 800 °C for three days in a cyclic heating mode. Physical shape of the samples can be readily seen in Fig. 3 after each cycle at the three oxidation temperatures of this study. The oxide growth at 800 °C can be easily seen after only one cycle even at the macro level. However, the oxidation at 600 and 700 °C appears to be quite reasonable in the sense that the development of an oxide-metal interface is quite apparent. The samples after static oxidation for 12 and 24 h at both 600 and 800 °C have been presented in Fig. 3 for comparison. Static oxidation after 24 h at 800 °C clearly shows the outward growth of oxides at the faces of the cubed samples. The oxide details identification will be subject of another report to be published later.

The shape of the curve has been commonly related to the oxidation mechanisms. A linear curve between the mass gain per unit surface area and time is normally associated with the fact that the alloy does not form a protective oxide film and results in continuous oxidation at a constant rate. One possibility is the localized corrosion taking place allowing the oxidation to continuously take place in the unprotected areas of the metal. On the other hand, the parabolic oxidation curves are considered to be a result of the ions or electrons penetrating through the oxide film, the rate controlling process, and hence the rate of oxidation decreases continuously as the oxide layer thickness increases. Lastly, a logarithmic rate law assumes that there is a transfer of electrons through the oxide film. Oxidation process is either the movement of ions inwards into the metal or ions moving outwards to the surface exposed to the oxidizing atmosphere. In Cr, Co, Ni, Cu and Fe cations move outwards in the diffusion process while in refractory metals like Nb, Ti, Hf and Ta, the anions O^{-2} move inwards [30].

3.3. Static oxidation

The results of isothermal heating at temperatures ranging from 600 to 1400 °C for 12 and 24 h is shown in Fig. 4. Curves shown in this figure clearly indicate that mass gain per unit surface area is more for 24 h of heating time, an, obviously, expected behavior. Fig. 4 shows a parabolic oxidation in this high entropy alloy. Thus it would indicate that the oxidation involves a gradual process of oxide patch formation resulting in continuous decreasing oxidation rate until the metal surface is completely covered with the oxide/oxides. Higher mass gain per unit surface area at periods of heating time (24 h) can thus be attributed to the prolonged diffusion process.

The authors have shown in their earlier research on Nb alloys that a selective oxidation may be prevalent at localized grains for a particular phase. Nature of this phase producing preferential oxidation will have to be dependent on the system. Such an evidence in this HEA has not been observed thus far.

The effect of time of heating to the oxidation temperature on the mass gain per unit area has been studied in terms of heating rate. Fig. 5 demonstrates that the heating rate does not appear to be a factor contributing to the oxidation process. However, it must be noted that the differences in the two heating rates, 3 and 10 °C per minute, may not be large enough to generalize such effects.

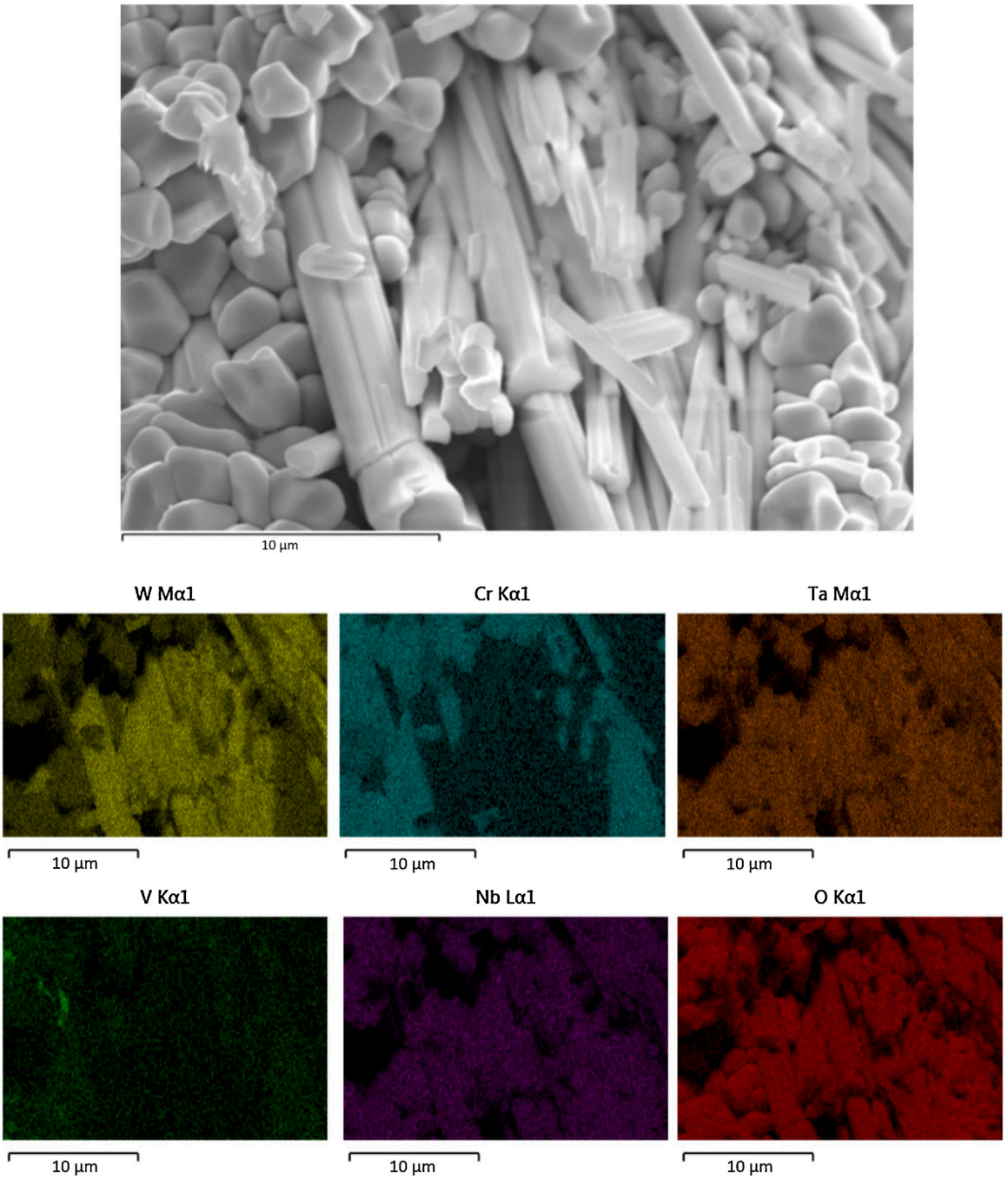

Fig. 7. X-ray mapping for the microstructures of the oxides developed at 1000 °C for 24 h. Crystals of various oxides can be seen.

Physical shapes of the, initially cubic, alloy samples after static oxidation are shown in Fig. 6 for samples subjected to 12 and 24 h of isochronal heating in a range of temperature from 600 to 1400 °C when the heating rate to the oxidation temperature was 3°/min. The alloy completely oxidizes beyond 1000 °C leaving no traces of metal left. This was the reason why detailed microstructural study involving the determination of the nature of oxide–metal interface could not be performed.

3.4. Oxide characterization

The characterization of the oxides formed in this alloy has been initiated. Some of the preliminary results will be presented here. Fig. 7 shows SEM results for the alloy oxidized at 1000 °C. The EDS has been used to map out the location and morphology of the various oxides that are formed. It must be noted from this figure that are two separate morphologies of oxides, (a) cylindrical and (b) granular or nodular. Elemental mapping indicated that the cylindrical shaped oxide crystals are the W and Ta oxide while nodules are oxides of Nb and Cr. V oxide is indicated by only a trace amount at this temperature.

Fig. 8 shows the oxide identification for the alloy at 1200 °C. Differences in the oxide morphologies include the (a) cylindrical, (b) nodular or granular, and (c) whiskers. The cylindrical and granular oxides are identical to those formed at 1000 °C. However, the presence of V oxide is much more noticeable at this temperature in whisker form. It appears that V oxide begins to form at temperatures at or above 1200 °C.

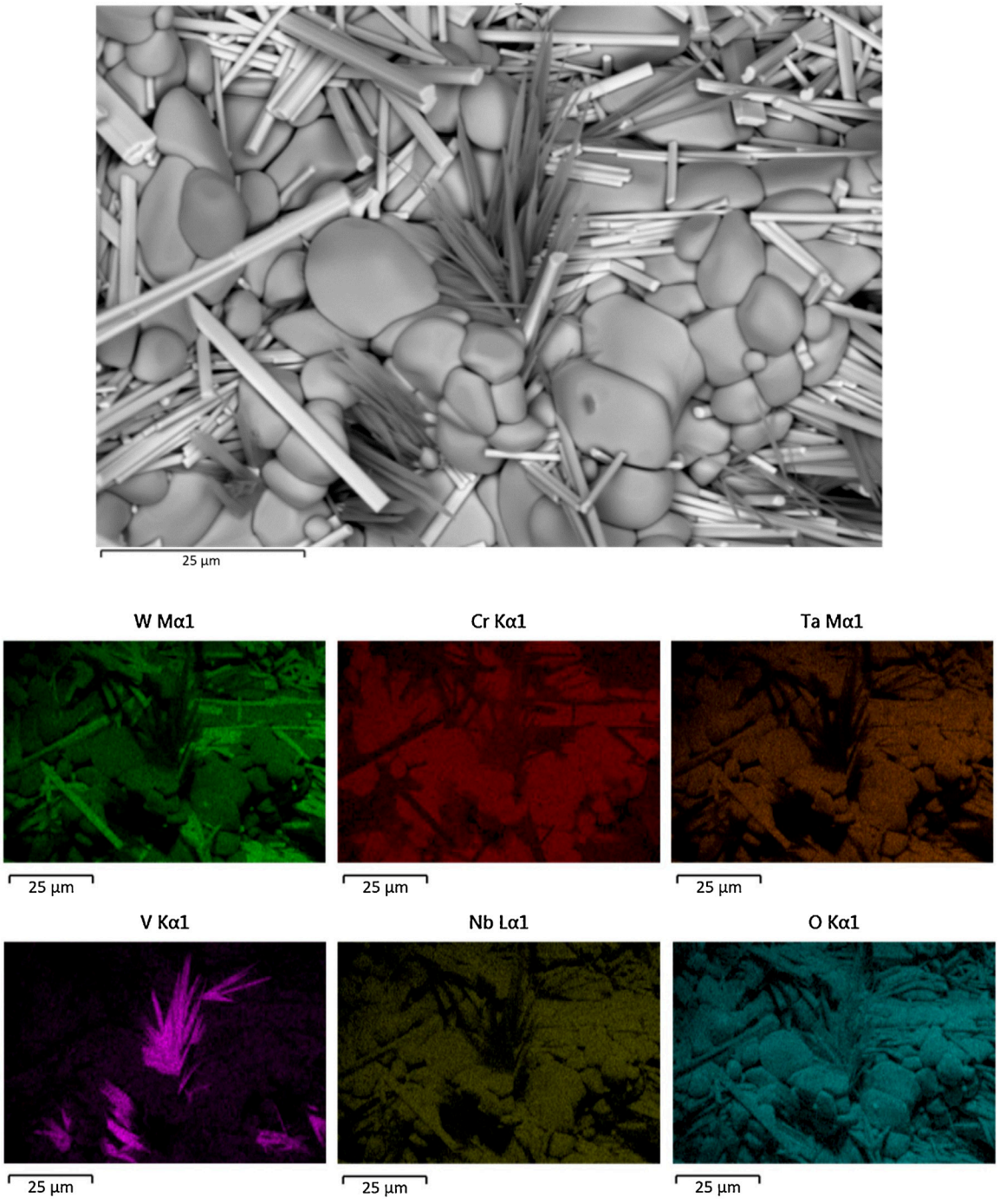

Fig. 8. X-ray mapping for the microstructures of the oxides developed at 1200 °C for 24 h. Crystals of various oxides can be seen.

The HEA phases can be either BCC or FCC [2]. The BCC unit cell may be envisioned to be a cube containing four different types of atoms at the corner positions on {001} planes while fifth atom occupies the body centered position for an HEA with 5 principal elements. On the other hand, FCC structure is such that {001} planes again contain 4 different atoms for the principal elements on the corners of the cube while the 6 face centered positions are occupied by the different atoms but one of the atoms would have to be repeated in such locations. It can be, nevertheless, seen that FCC lattices that are already quite densely packed with atoms are strained still further in this proposed structural configuration. However, either of these configurations allow us to explain the preferential oxides formed at the surfaces in layered structural form as shown in Fig. 5. The oxidation would begin to proceed at the lattice sites on the surface with a preferentially oxidizing atom of the metal. It can be assumed that the atom of the fifth element in the body centered position for BCC phase, for example, could concentrate at the surfaces, physically, in preferred grain orientations and thus cause the preferential oxidation of a given element at the surface. The detailed experimental verification of this hypothesis will be presented in a follow up study.

4. Conclusions

The conclusions derived based on the studies performed are:

(1) The Nb-Cr-V-W-Ta HEA of this study demonstrates that it is not capable of withstanding the oxidation temperatures higher than 1000 °C in air.
(2) A good oxidation resistance for this alloy has been observed at lower temperatures, 600, 700 and 800 °C, for 3 days in air.
(3) Oxides of W and Ta take up cylindrical shape crystallites while granular or nodular shapes of Nb and Cr oxides have been observed up to 1200 °C.
(4) Presence of V oxide appears to initiate only at 1200 °C with a whisker like morphology.

Acknowledgements

This work/manuscript is a contribution from Center for Advanced Materials Research (CMR). The authors acknowledge, with pleasure, support from the National Science Foundation with NSF-PREM grant #DMR-1827745.

References

[1] M.H. Tsai, J.W. Yeh, Mater. Res. Lett. 2 (2014) 107–123.
[2] Y. Zhang, T.T. Zuo, Z. Tang, Michael C. Gao, Karin A. Dahmen, Peter K. Liaw, Prog. Mater. Sci. 61 (2014) 1–93.
[3] Y.P. Lu, Y. Dong, S. Guo, L. Jiang, H. Kang, T.M. Wang, B. Wen, Z.J. Wang, J.C. Jie, Z.Q. Cao, H. Ruan, T.J. Li, Sci. Rep. 4 (6200) (2014) 1–5.
[4] D.B. Miracle, O.N. Senkov, Acta Mater. 122 (2017) 448–511.
[5] L. Santodonato, Y. Zhang, M. Feygenson, C.M. Parish, M.C. Gao, R.J.K. Weber, J.C. Neuefeind, Z. Tang, P.K. Liaw, Nat. Commn. 6 (2015) 5964.
[6] J. Zyka, J. Jarodlav, J. Vesely, F. Lukac, J. Cizek, J. Kuriplach, O. Melikhova, Entropy 21 (2019) 114.
[7] J. Yeh, S.K. Chen, J.W. Gan, S.J. Lin, T.S. Chin, T.T. Shin, C.H. Tasu, S.Y. Chang, Metall. Mater. Trans. A 35 (2004) 2533–2536.
[8] J. Yeh, S.K. Chen, J.W. Gan, S.J. Lin, T.S. Chin, T.T. Shin, C.H. Tasu, S.Y. Chang, Adv. Eng. Mater. 6 (2004) 299–303.
[9] J.W. Yeh, Ann. Chim. Sci. Mat. 31 (2006) 633–648.
[10] S. Guo, C. Ng, J. Lu, C.T. Liu, J. Appl. Phys. 109 (2011) 103–105.
[11] O.N. Senkov, G.B. Wilks, J.M. Scott, D.B. Miracle, Intermetallics 19 (2011) 698–706.
[12] O.N. Senkov, S.V. Senkova, C. Woodward, D.B. Miracle, Acta Mater. 61 (2013) 1545–1557.
[13] O.N. Senkov, S.V. Senkova, D.B. Miracle, C. Woodward, Mater. Sci. Eng. A 565 (2013) 51–62.
[14] J.M. Scott, S.V. Senkova, F. Meisenkothen, D.B. Miracle, J. Mater. Sci. 47 (2012) 4062–4074.
[15] O.N. Senkov, C.F. Woodward, Mater. Sci. Eng. A 529 (2011) 311–320.
[16] O.N. Senkov, J.M. Scott, S.V. Senkova, D.B. Miracle, C.F. Woodward, J. Alloys. Compd. 509 (2011) 6043–6048.
[17] O.N. Senkov, S.V. Senkova, D.B. Miracle, C. Woodward, Mater. Sci. Eng. A 565 (2013) 51–62.
[18] O.N. Senkov, F. Meisenkothen, D.B. Miracle, J. Mater. Sci. 47 (2012) 4062–4074.
[19] O.N. Senkov, J.M. Scott, S.V. Senkova, D.B. Miracle, C.F. Woodward, J. Alloys. Compd. 509 (2011) 6043–6048.
[20] M.H. Chuang, M.H. Tsai, W.R. Wang, S.J. Lin, J.W. Yeh, Acta Mater. 59 (2011) 6308–6317.
[21] C.Y. Hsu, C.C.Juan W.R. Wang, T.S. Sheu, J.W. Yeh, S.K. Chen, Mater. Sci. Eng. A 528 (2011) 3581–3588.
[22] W.H. Lin, Y. Wu, J.Y. He, T.G. Nieh, G.P. Lu, Scripta Mater. 68 (2013) 526–529.
[23] M.H. Tsai, H. Hang, G. Cheng, W. Xu, W.W. Jian, M.H. Chuang, C.C. Juan, A.C. Yeh, S.J. Lin, Y. Shu, Intermetallics 33 (2013) 81–86.
[24] T.T. Shun, C.H. Hung, C.F. Lee, J. Alloys. Compd. 495 (2010) 55–58.
[25] J.H. Perepezco, Science 326 (2009) 1068–1069.
[26] P.R. Subramanian, M.G. Mendiratta, D.M. Dimiduk, Mater. Sci. Eng. A 240 (1997) 1–13.
[27] B.P. Bewley, M.R. Jackson, J.-C. Zhao, P.R. Subramanian, Metal. Mater. Trans. A 34 (2003) 2043–2052.
[28] J.W. Yeh, Y.L. Chen, S.J. Lin, S.K. Chen, Mater. Sci. Forum 560 (2007) 109.
[29] J.W. Yeh, S.K. Chen, S.J. Lin, J.Y. Gan, T.S. Chin, T.T. Sun, C.H. Tsau, S.Y. Chang, Adv. Eng. Mater. 6 (2004) 299–303.
[30] M.G. Fontana, N.D. Green, Corrosion Engineering, Chapter 11, McGraw-Hill, New York, 1978.